

LETTER TO THE EDITOR

Discovery of the elusive radical NCO and confirmation of H_2NCO^+ in space [★]

N. Marcelino¹, M. Agúndez¹, J. Cernicharo¹, E. Roueff², and M. Tafalla³

¹ Instituto de Física Fundamental, CSIC, C/ Serrano 123, 28006 Madrid, Spain

² Sorbonne Université, Observatoire de Paris, Université PSL, CNRS, LERMA, F-92190, Meudon, France

³ Observatorio Astronómico Nacional (OAN), C/ Alfonso XII 3, 28014 Madrid, Spain

Received ; accepted

ABSTRACT

The isocyanate radical (NCO) is the simplest molecule containing the backbone of the peptide bond, $\text{C}(=\text{O})\text{-N}$. This bond has a prebiotic interest since is the one linking two amino acids to form large chains of proteins. It is also present in some organic molecules observed in space such as HNCO, NH_2CHO and CH_3NCO . In this letter we report the first detection in space of NCO towards the dense core L483. We also report the identification of the ion H_2NCO^+ , definitively confirming its presence in space, and observations of HNCO, HOCN, and HCNO in the same source. For NCO, we derive a column density of $2.2 \times 10^{12} \text{ cm}^{-2}$, which means that it is only ~ 5 times less abundant than HNCO. We find that H_2NCO^+ , HOCN and HCNO have abundances relative to HNCO of 1/400, 1/80, and 1/160, respectively. Both NCO and H_2NCO^+ are involved in the production of HNCO and several of its isomers. We have updated our previous chemical models involving NCO and the production of the CHNO isomers. Taking into account the uncertainties in the model, the observed abundances are reproduced relatively well. Indeed, the detection of NCO and H_2NCO^+ in L483 supports the chemical pathways to the formation of the detected CHNO isomers. Sensitive observations of NCO in sources where other molecules containing the $\text{C}(=\text{O})\text{-N}$ subunit have been detected could help in elucidating its role in prebiotic chemistry in space.

Key words. Astrochemistry – ISM: clouds, L483 – ISM: abundances – Stars: formation, low-mass Line: identification

1. Introduction

Most molecules observed in space can be formed with just four atoms, H, C, N, and O. These atoms are the building blocks of organic and prebiotic molecules, and arranged together, constitute the backbone of the peptide bond $\text{R}-\text{C}(=\text{O})-\text{N}(\text{H})-\text{R}'$, which links two amino acids and allows to build large proteins. Therefore, the observation of simple molecules with the $\text{C}(=\text{O})\text{-N}$ group in space can provide important clues on the earliest chemical steps in the synthesis of amino acids. The isocyanate radical (NCO) is the simplest such species and it is predicted to be abundant in dark clouds (Prasad & Huntress 1978; Marcelino et al. 2009). It is also the main precursor of isocyanic acid (HNCO), a species that has been found in a large variety of interstellar environments (see Marcelino et al. 2009, and references within).

HNCO has several metastable isomers: HOCN, HCNO, and HONC, which lie respectively at 24.7, 70.7, and 84.1 kcal mol⁻¹ respect to HNCO (see Schuurman et al. 2004). Two of these isomers, HCNO and HOCN, have also been previously detected in molecular clouds (Marcelino et al. 2009, 2010; Brünken et al. 2010). The chemical pathways to the formation of these species are diverse, but the main precursors in gas-phase are the radicals NCO and CNO (Marcelino et al. 2010; Quan et al. 2010). Followed by protonation and hydrogenation, these radicals will lead to the different protonated CHNO ions: H_2NCO^+ , HNCOH^+ , HCNOH^+ , H_2OCN^+ , and H_2CNO^+ (Marcelino et al. 2010; Quan et al. 2010). By dissociative recombination reactions, these ions

could produce all the CHNO isomers, including the highest isomer in energy HONC not detected so far in space, and also the NCO radical (Marcelino et al. 2010). The two isomeric forms of the protonated isocyanic acid H_2NCO^+ and HNCOH^+ , have been studied in the laboratory (Lattanzi et al. 2012; Gupta et al. 2013), and H_2NCO^+ has been tentatively detected in absorption of the low-lying rotational transitions in the centimeter band towards the molecular cloud Sgr B2(N) by Gupta et al. (2013).

In this letter, we report the first detection in space of NCO and we confirm the presence of H_2NCO^+ through millimeter emission transitions. These species were detected towards L483, a dense core located in the Aquila Rift which hosts a protostar, IRAS 18148–0440, in transition from Class 0 to Class I and which shows infall motions and a collimated molecular outflow (Tafalla et al. 2000; Park et al. 2000). Based on the bright emission of carbon chains like C_4H (Agúndez et al. 2008; Sakai et al. 2009), it has been suggested that L483 may host a warm-carbon-chain-chemistry environment. Apart from carbon chains, L483 is also rich in O-bearing organic molecules such as HCO, HCCO, H_2CCO , CH_3CHO , HCCCHO , and $c\text{-C}_3\text{H}_2\text{O}$ (Agúndez et al. 2015a; Loison et al. 2016). Recently, the chemical richness of the source has been evidenced with the discovery of several new molecules: HCCO, NCCNH^+ , NS^+ , HCS, and HSC (Agúndez et al. 2015a,b, 2018; Cernicharo et al. 2018). Recent ALMA observations have shown a chemical differentiation in L483, with carbon chains such as C_2H tracing the envelope and more complex organics like HNCO, NH_2CHO , and HCOOCH_3 being distributed around the protostar (Oya et al. 2017). The detection of NCO and H_2NCO^+ around a low-mass protostar such as L483 can thus shed light on the formation of prebiotic

[★] Based on observations carried out with the IRAM 30m telescope. IRAM is supported by INSU/CNRS (France), MPG (Germany) and IGN (Spain).

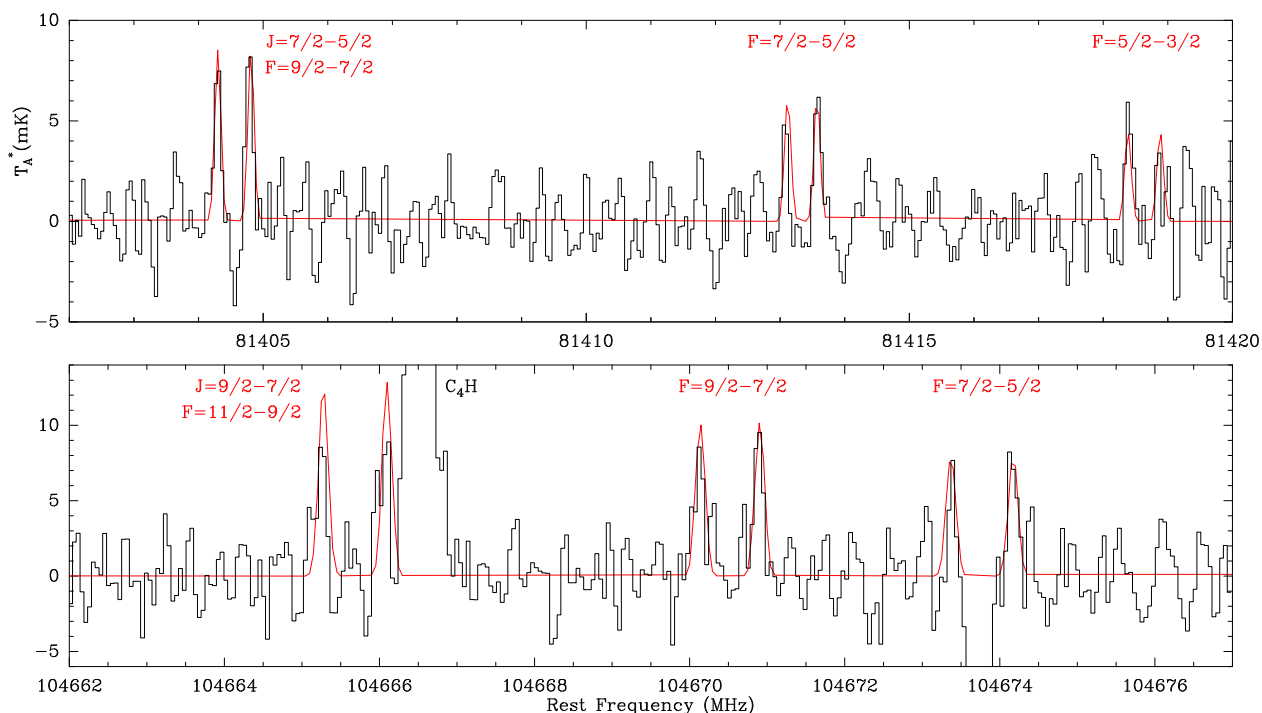


Fig. 1. Observed transitions of NCO in the $^2\Pi_{3/2}$ state towards L483. The strongest components of the $J = 7/2 - 5/2$ and $J = 9/2 - 7/2$ transitions are shown in the upper and lower panels, respectively. LTE results are overplotted in red. Note that the absorption feature in the lower panel between the doublet $F = 7/2 - 5/2$ is not real, it is the corresponding negative of the C_4H line due to the Frequency Switching observing mode (located 7.2 MHz away).

molecules containing the C(=O)–N group, like HNCO and its isomers, NH_2CHO , and CH_3NCO (Cernicharo et al. 2016; Qué-
nard et al. 2018).

2. Observations

The data presented here are part of a full 3 mm (80–116 GHz) spectral line survey of L483, using the IRAM 30m radiotelescope in Granada (Spain). The line survey observations were performed in several sessions, in August and November 2016, and in May and December 2017. We also obtained Director’s Discretionary Time to confirm the detection of NCO and H_2NCO^+ in January 2018. The observed position corresponds to that of the infrared source IRAS 18148–0440, $\alpha_{J2000} = 18^h17^m29.8^s$ and $\delta_{J2000} = -04^\circ39'38.0''$ (Fuller & Myers 1993).

We used the EMIR receivers operating at 3 mm, connected to the Fast Fourier Transform Spectrometers (FTS) in high resolution mode, providing a spectral resolution of 50 kHz, which corresponds to velocity resolutions of ~ 0.13 – 0.19 km s $^{-1}$ in the 80–116 GHz range. Thanks to the versatility of the EMIR and FTS, we could observe 4 different bands per spectral setup covering 4×1.8 GHz of bandwidth. All the observations were done in Frequency Switching mode, with a frequency throw of 7.2 MHz. Pointing and Focus were checked every 1 and 3 hours, respectively. Pointing errors were always within $3''$. The 30 m beam sizes at 3 mm are between $30''$ and $21''$. Weather conditions were different from one observing period to other, ranging from good winter conditions, with 2–5 mm of precipitable water vapor (pwv), to average summer conditions, with $pwv \leq 10$ mm. Concerning the data presented here, system temperatures range between 90 and 120 K and the final rms noise is ~ 1 – 4 mK, depending on frequency. The spectra were calibrated in antenna temperature corrected for atmospheric attenuation and for antenna ohmic and spillover losses using the ATM package (Cer-

nicharo 1985; Pardo et al. 2001). Data reduction and analysis were done using the CLASS program of the GILDAS software¹.

3. Results

During the analysis of the spectral survey data, we have found a number of unidentified lines. Among them there are several features at 81.4 GHz and 104.6 GHz which are coincident with the strongest components of the $J = 7/2 - 5/2$ and $J = 9/2 - 7/2$ transitions of the NCO radical in the $^2\Pi_{3/2}$ state (see Figure 1). The radical NCO is a linear triatomic molecule with a $^2\Pi_i$ electronic ground state, where the $^2\Pi_{1/2}$ spin-orbit state lies 137 K above the $^2\Pi_{3/2}$ state. The rotational levels are split by Λ doubling, leading to e and f parities, and are further split due to the interaction with the nuclear spin of ^{14}N , leading to a hyperfine structure (Saito & Amano 1970; Kawaguchi et al. 1985; see also CDMS²; Müller et al. 2005, and MADEX³; Cernicharo 2012). Already in 1978, this radical was predicted to be abundant in dark clouds (Prasad & Huntress 1978), although it has not been yet detected in space probably because of its low dipole moment (0.64 D, Saito & Amano 1970). The complex rotational spectrum of NCO helps in the assignment of the lines. The strongest components of the $J = 7/2 - 5/2$ and $J = 9/2 - 7/2$ are detected in L483, with no missing line, and with center frequencies and relative intensities in very good agreement with the values obtained from laboratory. With the identification of 12 different transitions, the detection of NCO can be considered secure.

We have also detected six lines arising from H_2NCO^+ , the lowest energy isomer of protonated isocyanic acid (see Figure 2). This ion has a large dipole moment (4.13 D, Lattanzi et al. 2012)

¹ <http://www.iram.fr/IRAMFR/GILDAS>

² <http://www.astro.uni-koeln.de/cdms/>

³ https://nanocosmos.iff.csic.es/?page_id=1619

Table 1. Column densities and fractional abundances derived.

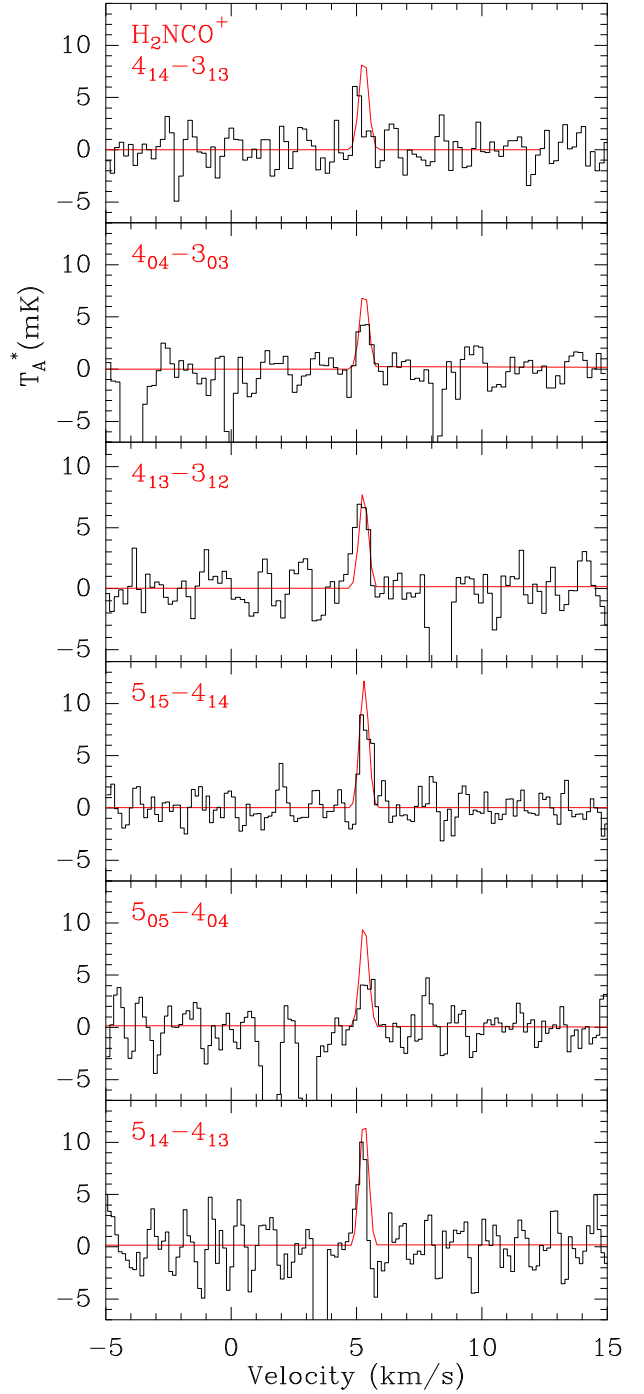
Species	N (cm^{-2})	X/H_2	HNCO/X
NCO	2.2×10^{12}	7.3×10^{-11}	5.5
H_2NCO^+	3.0×10^{10}	1.0×10^{-12}	400
HNCOH^+	$<2.3 \times 10^{10}$	$<7.7 \times 10^{-13}$	>520
HNCO	1.2×10^{13}	4.1×10^{-10}	–
HOCN	1.5×10^{11}	5.0×10^{-12}	80
HCNO	7.3×10^{10}	2.4×10^{-12}	160
HONC	$<8.3 \times 10^9$	$<2.8 \times 10^{-13}$	>1450

and has been tentatively detected towards the molecular clouds in the Galactic Center Sgr B2(N) in absorption at 20 and 40 GHz by Gupta et al. (2013). H_2NCO^+ is a planar molecular ion with a C_{2v} symmetry, in which the two H nuclei are equivalent. Thus, the rotational levels are separated into *ortho* (K_a odd) and *para* (K_a even) states, with statistical weights 3:1. Due to the ^{14}N nuclear spin, H_2NCO^+ also presents quadrupole hyperfine structure. However it is unresolved in the L483 spectra (see Fig. 2) and we do not take it into account in the analysis below. Although the lines of H_2NCO^+ in L483 are weak, with T_A^* between 5 and 10 mK, all of them are detected above the 3σ level (rms noise levels are 1.2–2 mK). Furthermore, the fact that all the strongest transitions covered in the 3 mm band are detected, well centered at the systemic velocity of L483 ($V_{\text{LSR}} \sim 5.3$ km s^{-1} ; Fuller & Myers 1993; Agúndez et al. 2008), supports the identification.

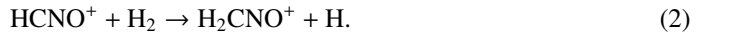
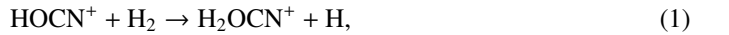
Table A.1 lists all the observed transitions, together with the line parameters derived from gaussian fits. Rest frequencies and spectroscopic data were taken from the MADEX catalogue (Cernicharo 2012). We have computed column densities assuming Local Thermodynamic Equilibrium (LTE) and $T_{\text{rot}} = 10$ K, which is consistent with the values obtained for other species in this cloud (Agúndez et al. 2015a,b). For NCO, since the range of upper level energies covered by the observed transitions is narrow (6.6–11.7 K; see Table A.1), the rotational temperature is poorly constrained using rotational diagrams. In the case of H_2NCO^+ , we have a relatively low number of transitions available when considering *ortho* and *para* species separately (in particular only two transitions are observed for the *para* state). Derived column densities are $N = (2.2 \pm 0.7) \times 10^{12} \text{ cm}^{-2}$ for NCO, and $3.0 \times 10^{10} \text{ cm}^{-2}$ for H_2NCO^+ (values for the *ortho* and *para* species are $(2.1 \pm 0.5) \times 10^{10} \text{ cm}^{-2}$ and $(8.6 \pm 3.9) \times 10^9 \text{ cm}^{-2}$, respectively). In the line survey we have also covered two transitions of HNCO, HOCN and HCNO. We have computed column densities for all these species assuming $T_{\text{rot}} = 10$ K. The fourth isomer, HONC, and the ion HNCOH^+ are not detected, and hence only upper limits are provided. The column densities and fractional abundances derived are listed for all species in Table 1. We used $N(\text{H}_2) = 3 \times 10^{22} \text{ cm}^{-2}$, which was derived by Tafalla et al. (2000) from observations of C^{17}O .

4. Discussion

The chemical processes linking H, C, O and N atoms take place in combustion processes but the kinetics at the low temperatures of interstellar clouds is subject to many uncertainties. To investigate the formation of NCO and H_2NCO^+ in L483, we have updated the chemical schema used in Marcelino et al. (2009, 2010) by considering the UMIST (McElroy et al. 2013) and KIDA (Wakelam et al. 2015) databases. In the absence of experimental or theoretical information on the kinetics, we have verified the energy balance of various reactions. Table A.2 reports our


Fig. 2. Observed transitions of H_2NCO^+ towards L483. LTE results are overplotted in red.

estimate of the formation enthalpies of different isomers of the CHNO^+ and CH_2NO^+ ions, which are not all reported in thermodynamic tables nor in the KIDA database. We find that some reactions suggested in KIDA are in fact endothermic, e.g.,



It is obvious that our tentative chemical network is subject to many uncertainties. Amongst these, the dissociative recombination (DR) rate coefficients of the CH_2NO^+ ions and the branch-

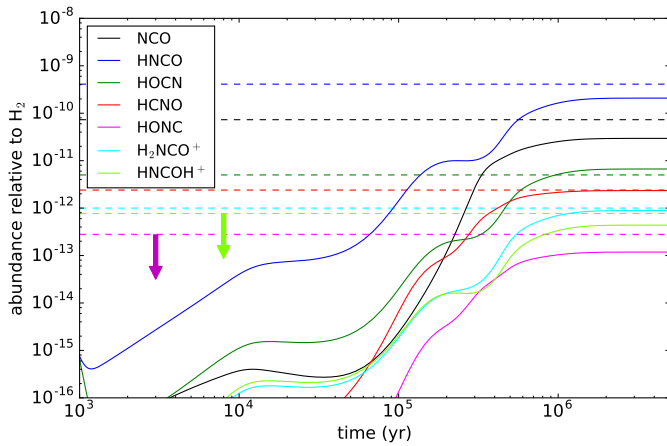


Fig. 3. Fractional abundances calculated as a function of time with our chemical model (see text). Horizontal dashed lines indicate the abundances derived from observations.

ing ratios are quite critical. The present model results are obtained when ejection of H and H₂ are favoured compared to other neutral channel products. In the cases where two CHNO isomers are produced in the DR, we have also assumed that the most stable is produced preferentially. The corresponding reaction rate coefficients are displayed in Table A.3. Another uncertainty in our chemical network is the formation route of H₂NCO⁺ through the NH₃ + HCO⁺ reaction, which is exothermic. For this channel we assume a rate coefficient of $2.5 \times 10^{-10} (T/300)^{-0.5} \text{ cm}^3 \text{ s}^{-1}$, while for the rapid proton transfer channel leading to NH₄⁺ + CO we consider a higher rate coefficient of $2.2 \times 10^{-9} (T/300)^{-0.5} \text{ cm}^3 \text{ s}^{-1}$.

In Fig. 3 we show the time evolution of the abundances of various species of interest, as given by our gas-phase chemical model. We have adopted a H₂ volume density of $3.4 \times 10^4 \text{ cm}^{-3}$ and a gas kinetic temperature of 10 K, which are adequate for the L483 cloud (Fuller & Myers 1993; Anglada et al. 1997; Jørgensen et al. 2002). The cosmic ionization rate is fixed to $1.3 \times 10^{-17} \text{ s}^{-1}$ and the elemental abundances of C, N, O, S relative to hydrogen are set to 9×10^{-6} , 1×10^{-5} , 1.5×10^{-5} and 2×10^{-8} , respectively. The relative abundances for the detected species are rather well reproduced by our model, while those of HONC and HNCOH⁺ are below the observed upper limits. Given the uncertainties of the chemical network, the agreement between the model and the observations is quite satisfactory.

The different species treated in this paper appear to follow different reaction routes, both through neutral-neutral reactions and ion-molecule schema. NCO is formed straightforwardly through the CN + O₂ reaction at a reaction rate of $2.4 \times 10^{-11} \text{ cm}^3 \text{ s}^{-1}$ (Glarborg et al. 1998). Fulminic acid (HCNO), despite at an energy of about 68 kcal mol⁻¹ above the most stable isomer HNCO, is one of the main products, together with HCN, of the reaction between CH₂ and NO, as found in the laboratory (Grussdorf et al. 1994) and explained theoretically (Rogenbuck & Temps 1998). HNCO and HOCN, on the other hand, are rather formed through ion molecule schema as products in the dissociative recombination of H₂NCO⁺ and HNCOH⁺, although the reaction for the latter has not yet been studied in the laboratory. The detection of H₂NCO⁺ validates the occurrence of the ion-molecule formation schema.

5. Conclusions

In this letter we report the first detection in space of the NCO radical with a significant abundance, only ~5 times lower than HNCO, towards the low-mass protostar L483. Together with H₂NCO⁺, detected as well in this dense core, they are involved in the production of HNCO and some of its isomers. In L483 we obtain similar abundances of HOCN and HCNO, which is consistent with what was found by Marcelino et al. (2010) in dense cores. It is possible that NCO and H₂NCO⁺ could be present in these sources as well. Unfortunately the corresponding frequencies were either not covered or the available data were not sensitive enough. Observations of NCO in sources at different stages across the star formation process could help to elucidate its role in the synthesis of CHNO isomers and prebiotic molecules containing the C(=O)–N group.

Acknowledgements. We thank the referee for his/her useful comments, and the IRAM 30m staff for their help during the observations and time allocation of the DDT project. We acknowledge funding support from the European Research Council (ERC Grant 610256: NANOCOSMOS) and from Spanish MINECO through grant AYA2016-75066-C2-1-P. M.A. also acknowledges funding support from the Ramón y Cajal programme of Spanish MINECO (RyC-2014-16277). E.R. acknowledges partial support by the French program “Physique et Chimie du Milieu Interstellaire” (PCMI) funded by the Conseil National de la Recherche Scientifique (CNRS) and Centre National d’Etudes Spatiales (CNES). M.T. acknowledges support from MINECO through grant AYA2016-79006-P.

References

- Agúndez, M., Cernicharo, J., Guélin, M., et al. 2008, *A&A*, 478, L19
 Agúndez, M., Cernicharo, J., & Guélin, M. 2015a, *A&A*, 577, L5
 Agúndez, M., Cernicharo, J., de Vicente, P., et al. 2015b, *A&A*, 579, L10
 Agúndez, M., Marcelino, N., Cernicharo, J., & Tafalla, M. 2018, *A&A*, 611, L1
 Anglada, G., Sepúlveda, I., & Gómez, J. F. 1997, *A&AS*, 121, 255
 Brünken, S., Belloche, A., Martín, S., Verheyen, L., & Menten, K. M. 2010, *A&A*, 516, A109
 Cernicharo, J. 1985, Internal IRAM report (Granada: IRAM)
 Cernicharo, J. 2012, in *ECLA-2011: Proc. of the European Conference on Laboratory Astrophysics*, EAS Publications Series, eds. C. Stehlé, C. Joblin, & L. d’Hendecourt (Cambridge: Cambridge Univ. Press)
 Cernicharo, J., Kiesel, Z., Tercero, B., et al. 2016, *A&A*, 587, L4
 Cernicharo, J., Lefloch, B., Agúndez, M., et al. 2018, *A&A*, 853, L22
 Fuller, G. A. & Myers, P. C. 1993, *ApJ*, 418, 273
 Glarborg, P., Alzueta, M. U., Dam-Johansen, K., & Miller, J. A. 1998, *Combustion and Flame*, 115, 1
 Grussdorf, J., Nolte, J., Temps, F., & Wagner, H. G. 1994, *Ber. Bunsenges. Phys. Chem.*, 98, 546
 Gupta, H., Gottlieb, C. A., Lattanzi, V., Pearson, J. C., & McCarthy, M. C. 2013, *ApJ*, 778, L1
 Ijjaali, F., Alcamí, M., Mó, O., & Yáñez, M. 2001, *Mol. Phys.*, 99, 1129
 Jørgensen, J. K., Schöier, F. L., & van Dishoeck, E. F. 2002, *A&AS*, 389, 908
 Kawaguchi, K., Saito, S., & Hirota, E. 1985, *Mol. Phys.*, 55, 341
 Lattanzi, V., Thorwirth, S., Gottlieb, C. A., & McCarthy, M. C. 2012, *J. Phys. Chem. Lett.*, 3, 3420
 Lias, S. G., Liebman, J. F., & Levin, R. D. 1984, *J. Phys. Chem. Ref. Data*, 13, 695
 Loison, J.-C., Agúndez, M., Marcelino, N., et al. 2016, *MNRAS*, 456, 4101
 Luna, A., Mebel, A. M., & Morokuma, K. 1996, *J. Chem. Phys.*, 105, 3187
 Marcelino, N., Cernicharo, J., Tercero, B., & Roueff, E. 2009, *ApJ*, 690, L27
 Marcelino, N., Brünken, S., Cernicharo, J., et al. 2010, *A&A*, 516, A105
 McElroy, D., Walsh, C., Markwick, A. J., et al. 2013, *A&A*, 550, A36
 Müller, H. S. P., Schlöder, F., Stutzki, J., & Winnewisser, G. 2005, *J. Mol. Struct.*, 742, 215
 Oya, Y., Sakai, N., Watanabe, Y., et al. 2017, *ApJ*, 837, 174
 Pardo, J. R., Cernicharo, J., & Serabyn, E. 2001, *IEEE Trans. Antennas Propag.*, 49, 12
 Park, Y.-S., Panis, J.-F., Ohashi, N., et al. 2000, *ApJ*, 542, 344
 Prasad, S. S., & Huntress, Jr., W. T. 1978, *MNRAS*, 185, 741
 Quan, D., Herbst, E., Osamura, Y., & Roueff, E. 2010, *ApJ*, 725, 2101
 Quénard, D., Jiménez-Serra, I., Viti, S., Holdship, J., Coutens, A. 2018, *MNRAS*, 474, 2796
 Rogenbuck, J., & Temps, F. 1998, *Chemical Physics Letters*, 285, 422
 Saito, S. & Amano, T. 1970, *J. Mol. Spectrosc.*, 34, 383
 Sakai, N., Sakai, T., Hirota, T., et al. 2009, *ApJ*, 697, 769
 Schuurman, M. S., Muir, S. R., Allen, W. D., & Shaefer III, H. F. 2004, *J. Chem. Phys.*, 120, 11586
 Tafalla, M., Myers, P. C., Mardones, D., & Bachiller, R. 2000, *A&A*, 359, 967
 Wakelam, V., Loison, J.-C., Herbst, E., et al. 2015, *ApJS*, 217, 20

Appendix A: Additional tables

Table A.1. Observed transitions and line parameters derived from Gaussian fits. Rest frequencies and spectroscopic data are taken from the MADEX catalogue (Cernicharo 2012).

Transition	Frequency (MHz)	E_{up} (K)	A_{ul} (s ⁻¹)	$\int T_A^* dv$ (mK km s ⁻¹)	V_{LSR} (km s ⁻¹)	Δv (km s ⁻¹)	T_A^* (mK)
NCO (²Π_{3/2})							
$J = 7/2 - 5/2 \quad F = 9/2 - 7/2 \quad e$	81404.300	6.6	$9.19 \cdot 10^{-7}$	3.6(9)	5.32(4)	0.42(10)	8.0
$J = 7/2 - 5/2 \quad F = 9/2 - 7/2 \quad f$	81404.813	6.6	$9.19 \cdot 10^{-7}$	4.1(9)	5.41(3)	0.42(7)	9.0
$J = 7/2 - 5/2 \quad F = 7/2 - 5/2 \quad e$	81413.120	6.6	$8.44 \cdot 10^{-7}$	2.1(9)	5.45(4)	0.34(10)	5.9
$J = 7/2 - 5/2 \quad F = 7/2 - 5/2 \quad f$	81413.573	6.6	$8.44 \cdot 10^{-7}$	3.2(9)	5.26(4)	0.45(10)	6.6
$J = 7/2 - 5/2 \quad F = 5/2 - 3/2 \quad e$	81418.385	6.6	$8.17 \cdot 10^{-7}$	2.9(9)	5.24(6)	0.44(11)	6.2
$J = 7/2 - 5/2 \quad F = 5/2 - 3/2 \quad f$	81418.884	6.6	$8.17 \cdot 10^{-7}$	1.6(9)	5.43(5)	0.27(17)	5.4
$J = 9/2 - 7/2 \quad F = 11/2 - 9/2 \quad e$	104665.278	11.7	$2.19 \cdot 10^{-6}$	5.0(9)	5.45(5)	0.55(10)	8.6
$J = 9/2 - 7/2 \quad F = 11/2 - 9/2 \quad f$	104666.098	11.7	$2.19 \cdot 10^{-6}$	5.4(9)	5.43(4)	0.55(7)	9.1
$J = 9/2 - 7/2 \quad F = 9/2 - 7/2 \quad e$	104670.139	11.7	$2.08 \cdot 10^{-6}$	3.6(9)	5.36(4)	0.45(11)	7.6
$J = 9/2 - 7/2 \quad F = 9/2 - 7/2 \quad f$	104670.905	11.7	$2.08 \cdot 10^{-6}$	3.9(9)	5.35(3)	0.37(8)	9.9
$J = 9/2 - 7/2 \quad F = 7/2 - 5/2 \quad e$	104673.371	11.7	$2.05 \cdot 10^{-6}$	1.6(9)	5.26(4)	0.22(7)	7.1
$J = 9/2 - 7/2 \quad F = 7/2 - 5/2 \quad f$	104674.173	11.7	$2.05 \cdot 10^{-6}$	2.9(9)	5.32(4)	0.35(8)	7.8
H₂NCO⁺							
$4_{1,4} - 3_{1,3}$	80246.376	8.7	$4.28 \cdot 10^{-5}$	2.0(5)	5.02(1)	0.18(60)	10.4
$4_{0,4} - 3_{0,3}$	80906.926	9.7	$4.67 \cdot 10^{-5}$	2.8(5)	5.32(5)	0.53(9)	4.9
$4_{1,3} - 3_{1,2}$	81565.636	8.8	$4.49 \cdot 10^{-5}$	4.9(9)	5.16(5)	0.63(10)	7.3
$5_{1,5} - 4_{1,4}$	100306.949	13.5	$8.74 \cdot 10^{-5}$	5.0(5)	5.37(3)	0.53(5)	8.9
$5_{0,5} - 4_{0,4}$	101131.130	14.6	$9.33 \cdot 10^{-5}$	3.8(9)	5.45(7)	0.70(15)	5.0
$5_{1,4} - 4_{1,3}$	101955.974	13.7	$9.18 \cdot 10^{-5}$	4.2(9)	5.20(4)	0.38(8)	10.4
HNCOH⁺							
$5 - 4$	99559.525	14.3	$8.82 \cdot 10^{-6}$	<0.8			<3.3
HNCO							
$4_{0,4} - 3_{0,3} \quad F = 3 - 3$	87924.381	10.5	$7.25 \cdot 10^{-7}$	19(1)	5.33(1)	0.33(2)	53.5
$4_{0,4} - 3_{0,3} \quad F = 5 - 4$	87925.252	10.5	$9.02 \cdot 10^{-6}$	761(2)	5.31(1)	0.44(1)	1619.6
$4_{0,4} - 3_{0,3} \quad F = 4 - 3$	87925.252	10.5	$8.46 \cdot 10^{-6}$				
$4_{0,4} - 3_{0,3} \quad F = 3 - 2$	87925.252	10.5	$8.29 \cdot 10^{-6}$				
$4_{0,4} - 3_{0,3} \quad F = 4 - 4$	87925.898	10.5	$5.64 \cdot 10^{-7}$	24(1)	5.30(1)	0.40(2)	57.4
$5_{0,5} - 4_{0,4} \quad F = 4 - 4$	109904.922	15.8	$8.81 \cdot 10^{-7}$	12(1)	5.33(1)	0.34(3)	33.2
$5_{0,5} - 4_{0,4} \quad F = 6 - 5$	109905.758	15.8	$1.80 \cdot 10^{-5}$	553(1)	5.31(1)	0.36(1)	1450.3
$5_{0,5} - 4_{0,4} \quad F = 5 - 4$	109905.758	15.8	$1.73 \cdot 10^{-5}$				
$5_{0,5} - 4_{0,4} \quad F = 4 - 3$	109905.758	15.8	$1.71 \cdot 10^{-5}$				
$5_{0,5} - 4_{0,4} \quad F = 5 - 5$	109906.430	15.8	$7.21 \cdot 10^{-7}$	11(1)	5.31(2)	0.37(4)	28.2
HO CN							
$4_{0,4} - 3_{0,3}$	83900.569	10.1	$4.18 \cdot 10^{-5}$	50(1)	5.31(1)	0.47(1)	99.7
$5_{0,5} - 4_{0,4}$	104874.676	15.1	$8.36 \cdot 10^{-5}$	34(1)	5.30(1)	0.38(1)	83.2
HCNO							
$4 - 3$	91751.320	11.0	$3.84 \cdot 10^{-5}$	21(1)	5.33(1)	0.41(2)	47.4
$5 - 4$	114688.383	16.5	$7.67 \cdot 10^{-5}$	8(2)	5.35(3)	0.26(5)	28.6
HONC							
$4 - 3$	87625.193	10.5	$3.41 \cdot 10^{-5}$	<2.1			<8.1
$5 - 4$	109530.044	15.8	$6.81 \cdot 10^{-5}$	<1.6			<6.9

Table A.2. Formation enthalpy estimates in kcal mol⁻¹

Species	ΔH	Ref.
HNCO ⁺	243	1
HOCN ⁺	274	2
HCNO ⁺	292	2
HONC ⁺	331.7	2
HNOC ⁺	331.4	2
H ₂ NCO ⁺	167	1
HNCOH ⁺	183	3
HCNOH ⁺	234.8	3
H ₂ OCN ⁺	240.9	3
H ₂ CNO ⁺	243	3

Notes. (1) Lias et al. (1984); (2) computed from Luna et al. (1996) using the experimental value for the most stable isomer HNCO⁺; (3) computed from Ijjaali et al. (2001) using the experimental value for the most stable isomer H₂NCO⁺.

Table A.3. Assumed rate coefficients of the DR reaction of the CH₂NO⁺ ions.

Reaction	Rate Coefficient ($\times 10^{-7} (T/300)^{-0.5} \text{ cm}^3 \text{ s}^{-1}$)
H ₂ NCO ⁺ + e → HNCO + H	2.50
H ₂ NCO ⁺ + e → CO + NH ₂	0.50
H ₂ NCO ⁺ + e → NCO + H ₂	1.50
H ₂ CNO ⁺ + e → HCNO + H	2.50
H ₂ CNO ⁺ + e → CH ₂ + NO	0.50
HCNOH ⁺ + e → HCNO + H	2.50
HCNOH ⁺ + e → HONC + H	0.50
HCNOH ⁺ + e → HCN + OH	0.50
HNCOH ⁺ + e → HOCN + H	0.50
HNCOH ⁺ + e → HNCO + H	2.50
HNCOH ⁺ + e → HNC + OH	0.50
H ₂ OCN ⁺ + e → HOCN + H	1.50
H ₂ OCN ⁺ + e → H ₂ O + CN	0.50